

Magnetoanisotropic Andreev Reflection in Ferromagnet/Superconductor Junctions

Petra Högl,¹ Alex Matos-Abiague,^{1,2} Igor Žutić,² and Jaroslav Fabian¹

¹*Institute for Theoretical Physics, University of Regensburg, 93040 Regensburg, Germany*

²*Department of Physics, University at Buffalo, State University of New York, Buffalo, NY 14260, USA*

Andreev reflection spectroscopy of ferromagnet/superconductor (FS) junctions is an important probe of spin polarization. We theoretically investigate spin-polarized transport in FS junctions in the presence of Rashba and Dresselhaus interfacial spin-orbit fields and show that Andreev reflection can be controlled by changing the magnetization orientation. We predict a giant in- and out-of-plane magnetoanisotropy of the junction conductance. If the ferromagnet is highly spin polarized—in the half-metal limit—the magnetoanisotropic Andreev reflection depends universally on the spin-orbit fields only. Our results show that Andreev reflection spectroscopy can be used for sensitive probing of interfacial spin-orbit fields in a FS junction.

Spin-orbit coupling (SOC) is a key interaction in spintronics [1–3], allowing an electrical control of magnetization and, vice versa, a magnetic control of electrical current. In systems lacking space inversion symmetry—be it bulk, hybrid structures, junctions—SOC induces spin-orbit fields [1, 2] as an emergent phenomenon. We are in particular concerned here with interfacial spin-orbit fields which are believed to be behind a wealth of new phenomena, not existent or fragile in the bulk, such as the tunneling anisotropic magnetoresistance (TAMR) [4–7], interfacial spin-orbit torques [8], or Skyrmions [9].

Interfacial spin-orbit fields are also important in semiconductor/superconductor [10–13] and ferromagnet/superconductor (FS) junctions [14] for creating Majorana quasiparticle states. It is the latter junctions that we focus on. We investigate the interplay of magnetism and spin-orbit fields. We show that this interplay leads to marked anisotropies in the junction conductance with respect to the orientation of magnetization. The most robust is the out-of-plane anisotropy (plane being the interface), which arises from the omnipresent Rashba field [15]. A more subtle is the in-plane anisotropy, which arises from the interference between the Rashba and Dresselhaus [16] fields, induced by a twofold anisotropy of the C_{2v} type. A zinc-blende semiconductor (say, GaAs or InAs) as a barrier in an FS junction would create such an anisotropy, generating spin-orbit fields C_{2v} “butterfly” patterns, as shown by first-principles calculations [17]. Remarkably, the resulting magnetoconductance anisotropy—we term it *magnetoanisotropic Andreev reflection (MAAR)*—is giant in comparison to TAMR, its normal-state counterpart, reaching a universal behavior in the half-metallic case. This is because Andreev reflection (AR) (which has no counterpart in the normal-state TAMR) is strongly influenced by interfacial spin-orbit fields.

We specifically examine the influence of SOC and crystalline anisotropy on the process of AR in which the reflected particle carries the information about both the phase of the incident particle and the macroscopic phase of the superconductor to which a Cooper pair is being transferred [18]. AR is thus responsible for the proximity

effect in which the phase correlations are introduced to a nonsuperconducting material [19–23]. While the main interest in AR is currently the proximity effect coupled with SOC, inducing Majorana states, in spintronics AR is used to probe the spin polarization in FS junctions [18–34]. We argue that AR can also be a sensitive probe of interfacial spin-orbit fields.

Our model FS junction consists of F ($z < 0$) and S ($z > 0$) semi-infinite regions separated by a flat interface at $z = 0$, with potential and SOC scattering. The scheme and possible scattering channels are illustrated in Fig. 1. For example, in conventional AR the incoming electron is reflected as a hole with the opposite spin, while spin-flip AR implies equal spin of the incoming and reflected particles. These two AR processes, see Figs. 1(b) and 1(f), introduce, respectively, spin-singlet and spin-triplet superconducting correlations at the interface [22, 23].

We consider epitaxial-quality junctions, such as those used in TAMR [6], or point contact geometries [35], in which ballistic transport formalism is applicable. In diffusive tunnel junctions AR could be enhanced by electron-hole coherence [36]. In ferromagnetic junctions such effects would be absent for normal AR due to short coherence length, but spin-flip AR could be enhanced. (Ordinary effects of diffusion could be accounted for by renormalizing the tunneling parameters [32]). We generalize the Blonder-Tinkham-Klapwijk formalism [37] and solve the Bogoliubov-de Gennes equation [38] for quasiparticle states $\Psi(\mathbf{r})$ with energy E ,

$$\begin{pmatrix} \hat{H}_e & \hat{\Delta} \\ \hat{\Delta}^\dagger & \hat{H}_h \end{pmatrix} \Psi(\mathbf{r}) = E \Psi(\mathbf{r}), \quad (1)$$

with the single-particle Hamiltonian for electrons $\hat{H}_e = -(\hbar^2/2)\nabla[1/m(z)]\nabla - \mu(z) - (\Delta_{xc}/2)\Theta(-z)\mathbf{m}\cdot\hat{\sigma} + \hat{H}_B$; for holes $\hat{H}_h = -\hat{\sigma}_y\hat{H}_e^*\hat{\sigma}_y$. The unit magnetization vector (see Fig. 1) is $\mathbf{m} = [\sin\Theta\cos\Phi, \sin\Theta\sin\Phi, \cos\Theta]$, $\hat{\sigma}$ are Pauli matrices, Δ_{xc} is the exchange spin splitting in the F region (Stoner model), $m(z)$ is the effective mass, and $\mu(z)$ is the chemical potential. The interfacial scattering is modeled as $\hat{H}_B = (V_0d + \mathbf{w}\cdot\hat{\sigma})\delta(z)$, where V_0 and d are the barrier height and width, while $\mathbf{w} =$

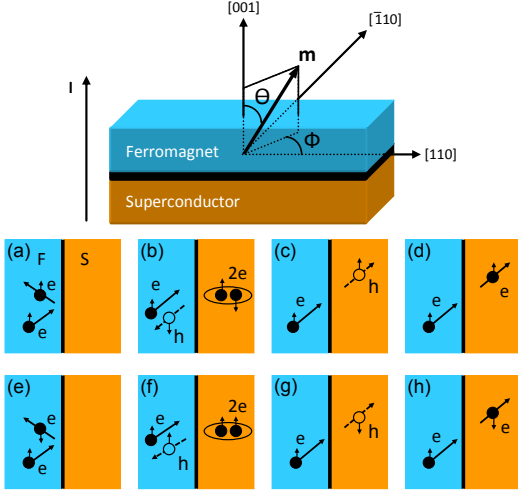


FIG. 1. (Color online) Top: FS junction. Magnetization vector \mathbf{m} is given by the polar angle Θ and azimuthal angle Φ . Current, I , flows perpendicular to the interface. To specify spin-orbit fields we use principal crystallographic orientations $x = [110]$, $y = [\bar{1}10]$, and $z = [001]$. Bottom: Scattering processes at the FS interface with SOC. Electrons (holes) are depicted by full (empty) circles. Vertical arrows denote the spin. The processes for a spin up incoming electron: (a) Specular reflection, (b) Andreev reflection, (c) holelike transmission, and (d) electronlike transmission. (e)-(h) Corresponding spin-flip counterparts. Spin-flip (equal electron and hole spins) Andreev reflection is in (f).

$[(\alpha - \beta)k_y, -(\alpha + \beta)k_x, 0]$ is the effective SOC field including Rashba and Dresselhaus terms [1, 2], parametrized by α and β , respectively, for the crystallographic orientations see Fig. 1. The superconducting pair potential is given by $\hat{\Delta} = \Delta\Theta(z)\mathbb{1}_{2 \times 2}$ (the accuracy of such a step-function form of $\hat{\Delta}$ is discussed in Ref. [39]), with the isotropic gap Δ . Similar methodology, for half-metal/S junctions with Rashba coupling inside the superconductor was employed in Ref. [40]. With Rashba-only SOC one should still obtain out-of-plane magnetoanisotropy, and this is already implicit in this formalism [40].

Since the in-plane wave vector \mathbf{k}_{\parallel} is conserved, $\Psi_{\sigma}(\mathbf{r}) = \Psi_{\sigma}(z)e^{i\mathbf{k}_{\parallel}\mathbf{r}_{\parallel}}$. The solution in the F region for incoming electrons with spin σ is

$$\Psi_{\sigma}^F = \frac{1}{\sqrt{k_{\sigma}^e}} e^{ik_{\sigma}^e z} \chi_{\sigma}^e + r_{\sigma,\sigma}^e e^{-ik_{\sigma}^e z} \chi_{\sigma}^e + r_{\sigma,-\sigma}^e e^{-ik_{-\sigma}^e z} \chi_{-\sigma}^e + r_{\sigma,-\sigma}^h e^{ik_{-\sigma}^h z} \chi_{-\sigma}^h + r_{\sigma,\sigma}^h e^{ik_{\sigma}^h z} \chi_{\sigma}^h, \quad (2)$$

with the spinors for the electronlike $\chi_{\sigma}^e = (\chi_{\sigma}, 0)^T$ and holelike $\chi_{\sigma}^h = (0, \chi_{-\sigma})^T$ quasiparticles, both containing

$$\chi_{\sigma}^T = (\sigma\sqrt{1 + \sigma \cos \Theta} e^{-i\Phi}, \sqrt{1 - \sigma \cos \Theta}) / \sqrt{2}, \quad (3)$$

where $\sigma = 1(-1)$ corresponds to the spin parallel (antiparallel) to $\hat{\mathbf{m}}$. The electronlike (holelike) quasiparticle wave vectors in the F region are $k_{\sigma}^{e(h)} = \sqrt{k_F^2 + 2m_F/\hbar^2 [(-)E + \sigma\Delta_{xc}/2]} - k_{\parallel}^2$.

In the S region the scattering states are

$$\Psi_{\sigma}^S = t_{\sigma,\sigma}^e e^{iq^e z} \begin{pmatrix} u \\ 0 \\ v \end{pmatrix} + t_{\sigma,-\sigma}^e e^{iq^e z} \begin{pmatrix} 0 \\ u \\ v \end{pmatrix} + t_{\sigma,\sigma}^h e^{-iq^h z} \begin{pmatrix} v \\ 0 \\ u \end{pmatrix} + t_{\sigma,-\sigma}^h e^{-iq^h z} \begin{pmatrix} 0 \\ v \\ u \end{pmatrix}, \quad (4)$$

where the quasiparticle wave vectors are given by $q^{e(h)} = \sqrt{q_F^2 + (-)2m_S/\hbar^2 \sqrt{E^2 - \Delta^2} - k_{\parallel}^2}$. The superconducting coherence factors satisfy $u^2 = 1 - v^2 = (1 + \sqrt{E^2 - \Delta^2}/E)/2$.

Using charge current conservation, the differential conductance at zero temperature, normalized by the Sharvin conductance [1] $G_{Sh} = e^2 k_F^2 A / (2\pi\hbar)$ of a perfect contact, is

$$G = \sum_{\sigma} \int \frac{d^2 \mathbf{k}_{\parallel}}{2\pi k_F^2} [1 + R_{\sigma}^h(-eV) - R_{\sigma}^e(eV)], \quad (5)$$

containing the probability amplitudes in the F region $R_{\sigma}^{e(h)}(E, \mathbf{k}_{\parallel}) = \text{Re} \left(k_{\sigma}^{e(h)} \left| r_{\sigma,\sigma}^{e(h)} \right|^2 + k_{-\sigma}^{e(h)} \left| r_{\sigma,-\sigma}^{e(h)} \right|^2 \right)$ which combine the coefficients for the scattering processes with and without spin flip for specular reflection and AR; V is the bias voltage and A is the interfacial area.

To describe our results we introduce dimensionless quantities: $Z = V_0 d \sqrt{m_F m_S} / (\hbar^2 \sqrt{k_F q_F})$ denotes the barrier strength [31, 37], $\lambda_{\alpha} = 2\alpha \sqrt{m_F m_S} / \hbar^2$ and $\lambda_{\beta} = 2\beta \sqrt{m_F m_S} / \hbar^2$ quantify the Rashba and Dresselhaus SOC, and $P = (\Delta_{xc}/2) / \mu_F$ defines the spin polarization in F.

We first examine the influence of SOC on the FS conductance (see Fig. 2), for a metallic point contact ($Z = 0$) and for a moderate barrier ($Z = 1$). For the former case the conductance tends to decrease with increasing SOC. Even in the half-metallic case ($P = 1$) SOC does not give a finite subgap conductance; spin-flip AR is suppressed. In contrast, for moderate barrier ($Z = 1$), SOC enhances the conductance due to spin-flip AR, even for $P = 1$. Interestingly, at $eV = \Delta$ the conductance is not affected by SOC for any Z . Focusing on $G(0)$, Fig. 2 shows that in a metallic contact increasing SOC steadily reduces $G(0)$, while for a moderate barrier $G(0)$ is a non-monotonic function of SOC, with a (P -dependent) maximum which turns out to be due to spin-flip AR.

The absence of spin-flip AR in metallic contacts can be explained analytically. For $eV \leq \Delta$ quasiparticle transmission is prohibited and subgap conductance $G \sim \sum_{\sigma} \int d^2 \mathbf{k}_{\parallel} 2R_{\sigma}^h(-eV)$. In the half-metallic case the only contribution to AR comes from spin-flip AR, $R_{\sigma}^h(E) = \text{Re} \left(k_{\sigma}^h \left| r_{\sigma,\sigma}^h \right|^2 \right)$, because of the missing minority spin subband in F. To lowest order in SOC and

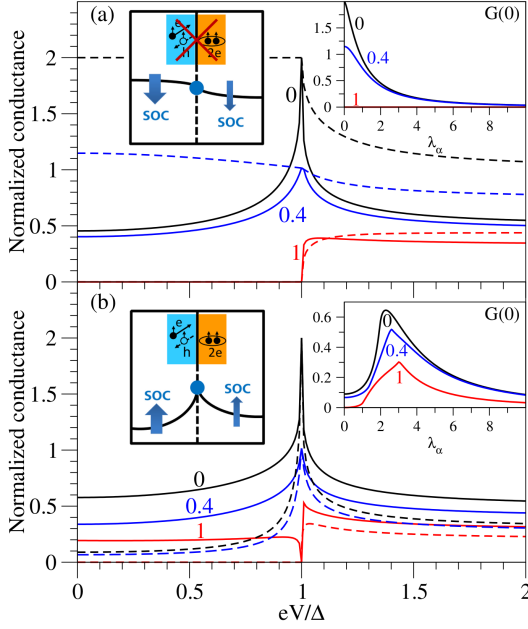


FIG. 2. (Color online) Calculated normalized conductance, $G(eV/\Delta)$, for different (indicated) spin polarizations P . Rashba SOC is $\lambda_\alpha = 2$ and Dresselhaus SOC is $\lambda_\beta = 0$. Magnetization is in plane ($\Theta = \pi/2$). (a) No interfacial barrier ($Z = 0$), and (b) modest interfacial barrier ($Z = 1$) cases are shown. The dashed lines show G without SOC. The insets show the dependence of $G(0)$ on Rashba SOC. In (a), the subgap conductance for $P = 1$ vanishes for every $\lambda_{\alpha,\beta}$; in the inset $G(0) = 0$ for this case. The illustrations summarize main qualitative impacts of SOC on conductance.

Z then $G(0) \propto Z^2 \lambda_i^2$ with $i \in \{\alpha, \beta\}$ [41], vanishing if $Z = 0$. This perturbative quadratic dependence on the spin-orbit strength was also obtained in Ref. [40].

The calculated conductance features of SOC [42–46] can be distinguished from k -independent spin-flip scattering by magnetic moments: For $Z = 0$ SOC always reduces the conductance and the subgap conductance vanishes for $P = 1$. In contrast, k -independent spin-flip scattering [47] can increase the conductance and the subgap conductance is in general finite for $P = 1$. However, similar features as those of SOC can arise in exotic superconductors without bulk inversion symmetry [48].

While the conductance changes are indicative of interfacial SOC, magnetic anisotropy of the conductance is a true fingerprint. As the main contribution comes from AR, we call this anisotropy effect *magnetoanisotropic Andreev reflection*. We consider two configurations: in plane, in which magnetization \mathbf{m} changes azimuthally (Φ) in the interfacial plane, and out of plane, with polar (Θ) changes of \mathbf{m} in a perpendicular plane (see Fig. 1). We define the in-plane MAAR as

$$\text{MAAR}_{[110]}(\Phi) = \frac{G(\Theta, 0) - G(\Theta, \Phi)}{G(\Theta, \Phi)} \Big|_{\Theta=90^\circ}, \quad (6)$$

and the out-of-plane MAAR as

$$\text{MAAR}_{[1\bar{1}0]}(\Theta) = \frac{G(0, \Phi) - G(\Theta, \Phi)}{G(\Theta, \Phi)} \Big|_{\Phi=-90^\circ}. \quad (7)$$

The out-of-plane MAAR depends, in general on Φ , but we choose the yz ($\Phi = -90^\circ$) plane as its reference.

The calculated MAAR, in Fig. 3, shows a nonmonotonic dependence on SOC. For metallic contacts ($Z = 0$) MAAR is determined by the magnetoanisotropy of conventional AR. In the presence of a barrier (exemplified by $Z = 1$), MAAR gets strongly enhanced due to the additional contribution from spin-flip AR. In-plane MAAR exhibits C_{2v} symmetry due to the interplay of Rashba and Dresselhaus fields, similarly to TAMR [2, 6, 7]. If either of the two fields is absent, in-plane MAAR vanishes. In contrast, out-of-plane MAAR is finite even with the Rashba field alone, which makes it a robust probe of this important interfacial SOC. Interestingly, at $eV = \Delta$ MAAR is always absent, as there are no effects of SOC on G here; see the discussion to Fig. 2. Additional effects (such as appearance of symmetry lobes) can arise due to the effective mass and Fermi wave vector mismatch [41].

Compared to TAMR, the magnitude of MAAR is giant, varying by orders of magnitude upon changing the spin polarization P . (The experimentally measured in-plane TAMR in Fe/GaAs/Au junctions is less than a per-

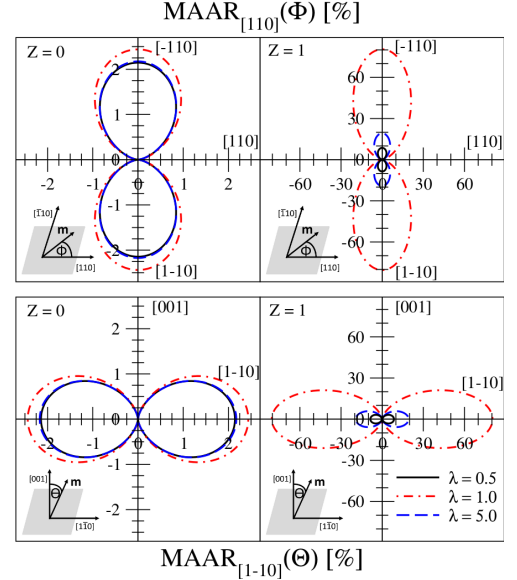


FIG. 3. (Color online) Top: Calculated in-plane magnetoanisotropic Andreev reflection (MAAR) with $[110]$ crystallographic reference axis for $Z = 0$ (left) and $Z = 1$ (right) for different strengths of SOC $\lambda_\alpha = \lambda_\beta = \lambda$ at $P = 0.4$ and $V = 0$. Bottom: Out-of-plane MAAR with $[1\bar{1}0]$ crystallographic reference axis. For $Z = 0$ the lines of $\lambda = 0.5$ and $\lambda = 5.0$ coincide. For the chosen reference axes and $\lambda_\alpha = \lambda_\beta$ the in-plane and out-of-plane MAAR curves have the same magnitude and shape, but rotated to the corresponding reference axis.

cent [6].) A detailed model comparison is shown in Fig. 4 for both in- and out-of-plane configurations; TAMR is evaluated by setting $\Delta = 0$. For a typical P of 40%, the ratio MAAR/TAMR is about 10. Moving towards half metals ($P \gtrsim 80\%$), this ratio climbs to more than 10^2 . This giant increase is best illustrated in the half-metallic limit of $P = 1$. For a weak SOC (which is typically the case) an analytical treatment gives [41],

$$\text{MAAR}_{[110]}(\Phi) \approx \frac{2\lambda_\alpha\lambda_\beta(1 - \cos 2\Phi)}{\lambda_\alpha^2 + \lambda_\beta^2 + 2\lambda_\alpha\lambda_\beta \cos 2\Phi}, \quad (8)$$

$$\text{MAAR}_{[1\bar{1}0]}(\Theta) \approx \frac{(\lambda_\alpha + \lambda_\beta)^2(1 - \cos 2\Theta)}{3(\lambda_\alpha^2 + \lambda_\beta^2) - 2\lambda_\alpha\lambda_\beta + (\lambda_\alpha + \lambda_\beta)^2 \cos 2\Theta}. \quad (9)$$

Therefore, the in-plane $\text{MAAR}_{[110]}(\Phi = \pi/2) \approx 4\lambda_\alpha\lambda_\beta/(\lambda_\alpha - \lambda_\beta)^2$, and out-of-plane $\text{MAAR}_{[1\bar{1}0]}(\Theta = \pi/2) \approx (\lambda_\alpha + \lambda_\beta)^2/(\lambda_\alpha - \lambda_\beta)^2$, depending *universally on the spin-orbit fields only*, and *diverging* as $\lambda_\alpha \approx \lambda_\beta$ (see the in-plane case in Fig. 4). In contrast, TAMR, which is proportional to the product $\lambda_\alpha\lambda_\beta$ [7], has no singular behavior, and is not a universal function of λ_i only.

We can trace this giant enhancement of MAAR over TAMR to spin-flip AR. Let us separate phenomenologically the conductance $G = G^{(0)} + G_{so}$ into the sum of SOC independent and dependent parts. In TAMR typically $G^{(0)} \gg G_{so}$, and $\text{TAMR} \sim G_{so}/G^{(0)} \ll 1$, even

for $P \approx 1$. But in FS junctions $G^{(0)}$ decreases with increasing P , eventually vanishing in the half-metallic limit. For $P \approx 1$ the conductance of the FS junction is dominated by the spin-flip AR contribution to G_{so} . Thus, SOC determines both the conductivity and the magnetoanisotropy. Furthermore, if $\lambda_\alpha \approx \pm\lambda_\beta$, the spin-flip AR, and so the conductance, can be switched *on* and *off* by changing the orientation of \mathbf{m} . For $\lambda_\alpha = \lambda_\beta$ and $\Phi = 0$, $\mathbf{m} \perp \mathbf{w}$ and spin-flip AR yields a finite G . However, if $\Phi = \pi/2$, then $\mathbf{m} \parallel \mathbf{w}$ and spin-flip processes are strongly suppressed; $G(eV \leq \Delta)$ at $\Phi = \pi/2$ vanishes. As a result, *in-plane MAAR diverges if $\lambda_\alpha = \lambda_\beta$* . Similarly for out-of-plane MAAR.

There is one more peculiarity of MAAR in the half-metallic limit. If only Rashba (or only Dresselhaus) SOC is present, out-of-plane MAAR has a *fixed universal* magnitude of 100%. This is shown in Fig. 4 (in particular the inset for $\lambda_i \lesssim 1$ shows MAAR of 100% for $P \approx 1$). It follows from Eq. (9) that $\text{MAAR}_{[1\bar{1}0]}(\Theta) \approx (1 - \cos 2\Theta)/(3 + \cos 2\Theta)$, which gives a universal amplitude of 100% for $\Theta = \pi/2$. In other words, $G(\Theta = 0) = 2G(\Theta = \pi/2)$. The origin of this universal behavior is traced to the spin-flip probability by scattering of spin-polarized electrons off spin-orbit fields. The conductance is determined by spin-flip AR. For out-of-plane magnetization, $\Theta = 0$, two fields, one along x and one along y , induce a spin flip. But for an in-plane magnetization, say along x , $\Theta = \pi/2$, only the spin-orbit field component along y can flip the spin. This gives the 2 : 1 ratio in conductances and 100% of MAAR. A more technical and detailed discussion of the differences between MAAR and TAMR can be found in Ref. 41.

Experimental realization of MAAR could follow the measurement geometry of TAMR [6], ideally also the same junction, with the nonmagnetic metal that becomes superconducting at low temperatures. Magnetization of the ferromagnetic layer is typically rotated by an external magnetic field. This field can bring additional anisotropic orbital effects whose presence can be clearly identified from the field magnitude dependence [49]. However, one can avoid these extrinsic effects entirely if one uses dysprosium magnets which can be oriented by the field, but do not need its presence to remain in the rotated position [50]. Potential aspects of nonflat tunneling barriers can also be treated [51]. A practical alternative (especially if ballistic junctions are desired) could be a point contact FS junction geometry [35, 52].

To conclude, we have applied a well-established theoretical formalism to systematically explore the magnetic anisotropy of the conductance in FS junctions due to interfacial SOC. We predict a giant in- and out-of-plane MAAR—when compared with TAMR—exhibiting universal characteristics in the half-metallic regime. The predicted magnetization control of the AR suggests a similar control of the superconducting proximity effect and Majorana states. Our findings reveal an unexplored

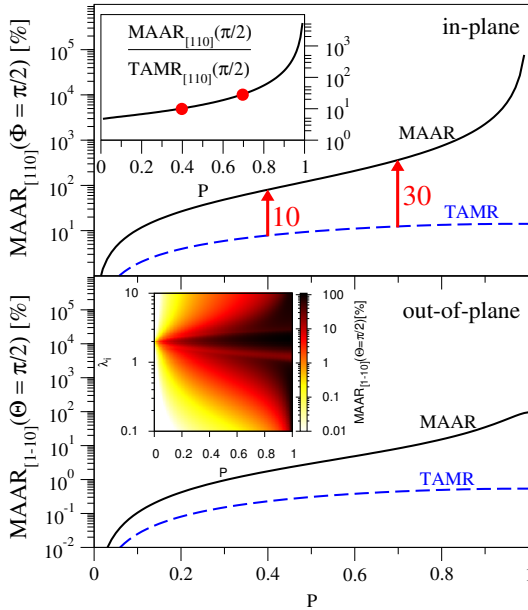


FIG. 4. (Color online) Calculated in-plane (top) and out-of-plane (bottom) MAAR and TAMR as a function of spin polarization P for a moderate barrier ($Z = 1$) and $V = 0$. The in-plane case is calculated with $\lambda_\alpha = \lambda_\beta = 1$, while for out of plane we have included Rashba $\lambda_\alpha = 0.5$ only. The top inset shows the ratio of MAAR and TAMR for the in-plane case, while the bottom inset shows the color map of out-of-plane MAAR as a function of P and Rashba (or Dresselhaus) SOC λ_i (where i could be either α or β).

venue for AR spectroscopy, in the sensitive probing of interfacial SOC and related magnetoanisotropic phenomena.

We acknowledge useful discussions with D. Weiss, C. Strunk, C. Back, B. Nadgorny, and P. Stamenov. This work has been supported by the DFG SFB 689, International Doctorate Program Topological Insulators of the Elite Network of Bavaria, DOE-BES Grant No. DE-SC0004890 (I.Ž.), and ONR N000141310754 (A.M.).

-
- [1] I. Žutić, J. Fabian, and S. Das Sarma, *Rev. Mod. Phys.* **76**, 323 (2004).
 - [2] J. Fabian, A. Matos-Abiague, C. Ertler, P. Stano, and I. Žutić, *Acta Phys. Slov.* **57**, 565 (2007).
 - [3] S. Maekawa, *Concepts in Spin Electronics* (Oxford University Press, Oxford, 2006).
 - [4] L. Brey, C. Tejedor, and J. Fernandez-Rossier, *Appl. Phys. Lett.* **85**, 1996 (2004).
 - [5] C. Gould, C. Rüster, T. Jungwirth, E. Girgis, G. M. Schott, R. Giraud, K. Brunner, G. Schmidt, and L. W. Molenkamp, *Phys. Rev. Lett.* **93**, 117203 (2004).
 - [6] J. Moser, A. Matos-Abiague, D. Schuh, W. Wegscheider, J. Fabian, and D. Weiss, *Phys. Rev. Lett.* **99**, 056601 (2007).
 - [7] A. Matos-Abiague and J. Fabian, *Phys. Rev. B* **79**, 155303 (2009); A. Matos-Abiague, M. Gmitra, and J. Fabian, *Phys. Rev. B* **80**, 045312 (2009).
 - [8] K. S. Ryu, L. Thomas, S. H. Yang, and S. Parkin, *Nat. Nanotechnol.* **8**, 527 (2013); A. Chernyshov, M. Overby, X. Liu, J. K. Furdyna, Y. Lyanda-Geller, and L. P. Rokhinson, *Nat. Phys.* **5**, 656 (2009).
 - [9] A. Fert, V. Cros, and J. Sampaio, *Nat. Nanotechnol.* **8**, 152 (2013).
 - [10] R. M. Lutchyn, J. D. Sau, and S. Das Sarma, *Phys. Rev. Lett.* **105**, 077001 (2010).
 - [11] Y. Oreg, G. Refael, and F. von Oppen, *Phys. Rev. Lett.* **105**, 177002 (2010).
 - [12] V. Mourik, K. Zuo, S. M. Frolov, S. R. Plissard, E. P. A. M. Bakkers, and L. P. Kouwenhoven, *Science* **336**, 1003 (2012).
 - [13] L. P. Rokhinson, X. Liu, and J. K. Furdyna, *Nat. Phys.* **8**, 795 (2012).
 - [14] S. Nadj-Perge, I. K. Drozdov, J. Li, H. Chen, S. Jeon, J. Seo, A. H. MacDonald, B. A. Bernevig, and A. Yazdani, *Science* **346**, 602 (2014).
 - [15] Y. A. Bychkov and E. I. Rashba, *J. Phys. C* **17**, 6039 (1984).
 - [16] G. Dresselhaus, *Phys. Rev.* **100**, 580 (1955).
 - [17] M. Gmitra, A. Matos-Abiague, C. Draxl, and J. Fabian, *Phys. Rev. Lett.* **111**, 036603 (2013).
 - [18] G. Deutscher, *Rev. Mod. Phys.* **77**, 109 (2005).
 - [19] A. I. Buzdin, *Rev. Mod. Phys.* **77**, 935 (2005).
 - [20] F. S. Bergeret, A. F. Volkov, and K. B. Efetov, *Rev. Mod. Phys.* **77**, 1321 (2005).
 - [21] A. A. Golubov, M. Y. Kupriyanov, and E. Il'ichev, *Rev. Mod. Phys.* **76**, 411 (2004).
 - [22] M. Eschrig, *Phys. Today* **64**, 43 (2011).
 - [23] C. Visani, Z. Sefrioui, J. Tornos, C. Leon, J. Briatico, M. Bibes, A. Barthélémy, J. Santamaría, and J. E. Villegas, *Nat. Phys.* **8**, 539 (2012).
 - [24] S. Kashiwaya and Y. Tanaka, *Rep. Prog. Phys.* **63**, 1641 (2000).
 - [25] M. J. M. de Jong and C. W. J. Beenakker, *Phys. Rev. Lett.* **74**, 1657 (1995).
 - [26] R. J. Soulen, J. M. Byers, M. S. Osofsky, B. Nadgorny, T. Ambrose, S. F. Cheng, P. R. Broussard, C. T. Tanaka, J. Nowak, J. S. Moodera, A. Barry, and J. M. D. Coey, *Science* **282**, 85 (1998).
 - [27] S. K. Upadhyay, A. Palanisami, R. N. Louie, and R. A. Buhrman, *Phys. Rev. Lett.* **81**, 3247 (1998).
 - [28] J.-X. Zhu, B. Friedman, and C. S. Ting, *Phys. Rev. B* **59**, 9558 (1999).
 - [29] S. Kashiwaya, Y. Tanaka, N. Yoshida, and M. R. Beasley, *Phys. Rev. B* **60**, 3572 (1999).
 - [30] I. Žutić and S. Das Sarma, *Phys. Rev. B* **60**, R16322 (1999).
 - [31] I. Žutić and O. T. Valls, *Phys. Rev. B* **60**, 6320 (1999); *Phys. Rev. B* **61**, 1555 (2000).
 - [32] I. I. Mazin, A. A. Golubov, and B. Nadgorny, *J. Appl. Phys.* **89**, 7576 (2001).
 - [33] K. Kikuchi, H. Imamura, S. Takahashi, and S. Maekawa, *Phys. Rev. B* **65**, 020508 (2001).
 - [34] C. S. Turel, I. J. Guilaran, P. Xiong, and J. Y. T. Wei, *Appl. Phys. Lett.* **99**, 192508 (2011).
 - [35] P. Stamenov, *J. Appl. Phys.* **111**, 07C519 (2012); *J. Appl. Phys.* **113**, 17C718 (2013).
 - [36] F. W. J. Hekking and Y. V. Nazarov, *Phys. Rev. Lett.* **71**, 1625 (1993).
 - [37] G. E. Blonder, M. Tinkham, and T. M. Klapwijk, *Phys. Rev. B* **25**, 4515 (1982).
 - [38] P. G. De Gennes, *Superconductivity of Metals and Alloys* (Addison-Wesley, Reading MA, 1989).
 - [39] C. W. J. Beenakker, *Rev. Mod. Phys.* **69**, 731 (1997).
 - [40] M. Duckheim and P. W. Brouwer, *Phys. Rev. B* **83**, 054513 (2011).
 - [41] See Supplemental Material at <http://link.aps.org/supplemental/10.1103/PhysRevLett.115.116601> for more details.
 - [42] L. P. Gor'kov and E. I. Rashba, *Phys. Rev. Lett.* **87**, 037004 (2001).
 - [43] Y. Mizuno, T. Yokoyama, and Y. Tanaka, *Phys. Rev. B* **80**, 195307 (2009).
 - [44] J. Linder and T. Yokoyama, *Phys. Rev. Lett.* **106**, 237201 (2011).
 - [45] F. Dolcini and L. Dell'Anna, *Phys. Rev. B* **78**, 024518 (2008).
 - [46] K. Sun and N. Shah, *Phys. Rev. B* **91**, 144508 (2015).
 - [47] A. V. Balatsky, I. Vekhter, and J.-X. Zhu, *Rev. Mod. Phys.* **78**, 373 (2006).
 - [48] S. Wu and K. V. Samokhin, *Phys. Rev. B* **80**, 014516 (2009); *Phys. Rev. B* **81**, 214506 (2010).
 - [49] M. Wimmer, M. Lobenhofer, J. Moser, A. Matos-Abiague, D. Schuh, W. Wegscheider, J. Fabian, K. Richter, and D. Weiss, *Phys. Rev. B* **80**, 121301 (2009).
 - [50] C. Bethhausen, T. Dollinger, H. Saarikoski, V. Kolkovsky, G. Karczewski, T. Wojtowicz, K. Richter, and D. Weiss, *Science* **337**, 324 (2012).
 - [51] Z. Y. Chen, A. Biswas, I. Žutić, T. Wu, S. B. Ogale, R. L. Greene, and T. Venkatesan, *Phys. Rev. B* **63**, 212508 (2001).
 - [52] J. Alicea, *Rep. Prog. Phys.* **75**, 076501 (2012).

SUPPLEMENTAL MATERIAL

Magnetoanisotropic Andreev Reflection in Ferromagnet/Superconductor Junctions

Petra Högl,¹ Alex Matos-Abiague,^{1,2} Igor Žutić,² and Jaroslav Fabian¹

¹*Institute for Theoretical Physics, University of Regensburg, 93040 Regensburg, Germany*

²*Department of Physics, University at Buffalo, State University of New York, Buffalo, NY 14260, USA*

(Dated: September 23, 2015)

TABLE S1. Dimensionless system parameters.

Z	barrier strength	$\frac{V_0 d \sqrt{m_F m_S}}{\hbar^2 \sqrt{k_F q_F}}$
λ_α	Rashba SOC	$2\alpha \sqrt{m_F m_S} / \hbar^2$
λ_β	Dresselhaus SOC	$2\beta \sqrt{m_F m_S} / \hbar^2$
P	spin polarization	$(\Delta_{xc}/2) / \mu_F$
F_K	Fermi wave vector mismatch	q_F / k_F
F_M	effective mass mismatch	m_S / m_F

BOUNDARY CONDITIONS

The reflection and transmission coefficients can be found by applying the following boundary conditions to the scattering states ensuring probability conservation

$$\Psi_\sigma^F|_{z=0^-} = \Psi_\sigma^S|_{z=0^+}, \quad (S1)$$

$$\begin{aligned} \frac{\hbar^2}{2m_S} \frac{d}{dz} \eta \Psi_\sigma^S|_{z=0^+} &= \begin{pmatrix} \mathbf{w} \cdot \hat{\boldsymbol{\sigma}} & 0 \\ 0 & -\mathbf{w} \cdot \hat{\boldsymbol{\sigma}} \end{pmatrix} \Psi_\sigma^F|_{z=0^-} \\ &+ \left(\frac{\hbar^2}{2m_F} \frac{d}{dz} + V_0 d \right) \eta \Psi_\sigma^F|_{z=0^-}, \end{aligned} \quad (S2)$$

where

$$\mathbf{w} = \frac{\hbar^2}{2\sqrt{m_F m_S}} \begin{pmatrix} (\lambda_\alpha - \lambda_\beta) k_y \\ -(\lambda_\alpha + \lambda_\beta) k_x \\ 0 \end{pmatrix}, \quad (S3)$$

represents the SOC field and η is

$$\eta = \begin{pmatrix} \mathbb{1}_{2 \times 2} & 0 \\ 0 & -\mathbb{1}_{2 \times 2} \end{pmatrix}. \quad (S4)$$

Equations (S1) and (S2) form a system of eight linear equations for determining the reflection and transmission coefficients.

ANALYTICAL RESULTS FOR $eV \leq \Delta$

In the energy range below the gap ($eV \leq \Delta$) transmission of quasiparticles is prohibited. Therefore, the probability coefficients for transmission are zero and probability current conservation gives $R_\sigma^h + R_\sigma^e = 1$ so that the normalized subgap conductance can be written as

$$G = \frac{1}{\pi} \sum_\sigma \int_0^{2\pi} d\varphi \int_0^{\sqrt{1+\sigma P}} dk k R_\sigma^h(-eV), \quad (S5)$$

where we introduce a dimensionless wave vector magnitude $k = k_\parallel / k_F$; φ is the polar angle. The probability coefficient for AR is defined as

$$R_\sigma^h(E, \mathbf{k}) = \text{Re} \left(k_\sigma^h |r_{\sigma,\sigma}^h|^2 + k_{-\sigma}^h |r_{\sigma,-\sigma}^h|^2 \right), \quad (S6)$$

To derive analytical results we apply Andreev approximation, i. e., we neglect corrections of the order $\mathcal{O}(E/\mu_{F,S}, \Delta/\mu_{F,S})$, with the chemical potential $\mu_{F,S}$ in the ferromagnet and in the superconductor, respectively. This leads to the wave vectors in F, $k_\sigma^e \approx k_\sigma^h \approx k_F k_\sigma$, with the dimensionless wave vector

$$k_\sigma = \sqrt{1 + \sigma P - k^2}. \quad (S7)$$

The superconducting wave vectors are $q^e \approx q^h \approx k_F q$ with the dimensionless wave vector

$$q = \sqrt{F_K^2 - k^2}. \quad (S8)$$

By inserting the scattering states to the boundary conditions [Eqs. (S1,S2)] we can obtain the scattering coefficients for AR with and without spin flip, respectively,

$$r_{\sigma,\sigma}^h = \sqrt{\frac{k_\sigma}{k_F}} \frac{-16F_M^2 q u v (u^2 - v^2) \sqrt{F_K} Z W_{\sigma,-\sigma}^*}{\Omega} \quad (S9)$$

and

$$\begin{aligned} r_{\sigma,-\sigma}^h &= \sqrt{\frac{k_\sigma}{k_F}} \frac{4F_M^2 q u v (u^2 + v^2) q (k_{-\sigma} + k_\sigma) + (u^2 - v^2) [q^2/F_M + F_M k_{-\sigma} k_\sigma - 2i\sqrt{F_M F_K} Z (k_{-\sigma} - k_\sigma) + 4F_K Z^2]}{\Omega} \\ &+ \sqrt{\frac{k_\sigma}{k_F}} \frac{4F_M^2 q u v (u^2 - v^2) \{ [i\sqrt{F_M} (k_{-\sigma} - k_\sigma) - 4\sqrt{F_K} Z] W_{\sigma,\sigma} + W_{\sigma,\sigma}^2 + W_{\sigma,-\sigma} W_{\sigma,-\sigma}^* \}}{\Omega} \end{aligned} \quad (S10)$$

with the denominator

$$\begin{aligned}
\Omega = & (u^2 - v^2)^2 \{q^4 + F_M^4 k_\sigma^2 k_{-\sigma}^2 + 4F_M^3 F_K Z^2 (k_\sigma^2 + k_{-\sigma}^2) + 16F_M^2 F_K^2 Z^4 + 8F_K F_M q^2 Z^2\} \\
& + (u^4 - v^4) 2q (k_\sigma + k_{-\sigma}) \{F_M q^2 + 4F_K F_M^2 Z^2 + F_M^3 k_\sigma k_{-\sigma}\} \\
& + (u^2 + v^2)^2 F_M^2 q^2 (k_\sigma^2 + k_{-\sigma}^2) + (u^4 + v^4) F_M^2 q^2 4k_\sigma k_{-\sigma} \\
& + W_{\sigma,\sigma} (u^4 - v^4) (k_{-\sigma}^2 - k_\sigma^2) 2iF_M^{5/2} q \\
& + W_{\sigma,\sigma} (u^2 - v^2)^2 (k_{-\sigma} - k_\sigma) \{2iF_M^{3/2} q^2 + 2iF_M^{7/2} k_{-\sigma} k_\sigma - 8iF_K F_M^{5/2} Z^2\} \\
& + (W_{\sigma,\sigma}^2 + W_{\sigma,-\sigma} W_{\sigma,-\sigma}^*) \{(u^4 - v^4) F_M^2 2q (k_\sigma + k_{-\sigma}) + (u^2 - v^2)^2 [-8F_M^2 F_K Z^2 + 2F_M q^2 + 2F_M^3 k_{-\sigma} k_\sigma]\} \\
& + (u^2 - v^2)^2 \{W_{\sigma,\sigma}^2 F_M^3 (-k_{-\sigma}^2 - k_\sigma^2 + 2k_\sigma k_{-\sigma}) + (W_{\sigma,\sigma}^3 + W_{\sigma,\sigma} W_{\sigma,-\sigma} W_{\sigma,-\sigma}^*) 2iF_M^{5/2} (k_{-\sigma} - k_\sigma)\} \\
& + (W_{\sigma,\sigma}^2 + W_{\sigma,-\sigma} W_{\sigma,-\sigma}^*)^2 (u^2 - v^2)^2 F_M^2.
\end{aligned} \tag{S11}$$

The dependence of the scattering coefficients on the orientation of magnetization is included in the SOC matrix elements $W_{\sigma,\pm\sigma}$. For in-plane magnetization ($\Theta = \pi/2$) they have the form

$$W_{\sigma,\sigma} = \sigma k [(\lambda_\alpha - \lambda_\beta) \sin \varphi \cos \Phi - (\lambda_\alpha + \lambda_\beta) \cos \varphi \sin \Phi] \tag{S12}$$

$$W_{\sigma,-\sigma} = i\sigma k [(\lambda_\alpha - \lambda_\beta) \sin \varphi \sin \Phi + (\lambda_\alpha + \lambda_\beta) \cos \varphi \cos \Phi]. \tag{S13}$$

For out-of-plane magnetization and $\Phi = -\pi/2$ the SOC matrix elements read

$$W_{\sigma,\sigma} = \sigma k (\lambda_\alpha + \lambda_\beta) \sin \varphi \sin \Theta \tag{S14}$$

$$W_{\sigma,-\sigma} = k (\lambda_\alpha + \lambda_\beta) \sin \varphi \cos \Theta + i\sigma k (\lambda_\alpha - \lambda_\beta) \cos \varphi. \tag{S15}$$

The spin-flip AR coefficient in Eq. (S9) can be rewritten as

$$r_{\sigma,\sigma}^h = aW_{\sigma,-\sigma}^* \left[b + cW_{\sigma,\sigma} + dW_{\sigma,\sigma}^2 + eW_{\sigma,-\sigma} W_{\sigma,-\sigma}^* + f(W_{\sigma,\sigma}^3 + W_{\sigma,\sigma} W_{\sigma,-\sigma} W_{\sigma,-\sigma}^*) + g(W_{\sigma,\sigma}^2 + W_{\sigma,-\sigma} W_{\sigma,-\sigma}^*)^2 \right]^{-1} \tag{S16}$$

where all the coefficients are functions of k .

ANALYTICAL RESULTS FOR HALF-METAL/S JUNCTION

In the case of a half metal ($P = 1$) the only contribution to AR comes from spin-flip AR because of the missing minority spin band in the half metal. Therefore, the AR probability coefficient becomes

$$R_\sigma^h(E) = \text{Re} \left[k_\sigma^h |r_{\sigma,\sigma}^h|^2 \right]. \tag{S17}$$

To derive analytical results for MAAR we neglect higher order SOC terms. To lowest order in SOC [$\mathcal{O}(\lambda_i^2)$] the spin-flip AR coefficient [Eq. (S16)] reduces to,

$$r_{\sigma,\sigma}^h \approx \frac{a(k)}{b(k)} W_{\sigma,-\sigma}^*. \tag{S18}$$

For weak SOC we can use Eqs. (S13,S17,S18) to obtain the following approximate expression for the in-plane MAAR for $eV < \Delta$

$$\text{MAAR}_{[110]}(\Phi) \approx \frac{2\lambda_\alpha \lambda_\beta (1 - \cos 2\Phi)}{\lambda_\alpha^2 + \lambda_\beta^2 + 2\lambda_\alpha \lambda_\beta \cos 2\Phi}. \tag{S19}$$

Analogously, we derive an expression for the out-of-plane

MAAR using Eq. (S15),

$$\text{MAAR}_{[1\bar{1}0]}(\Theta) \approx \frac{(\lambda_\alpha + \lambda_\beta)^2 (1 - \cos 2\Theta)}{3(\lambda_\alpha^2 + \lambda_\beta^2) - 2\lambda_\alpha \lambda_\beta + (\lambda_\alpha + \lambda_\beta)^2 \cos 2\Theta}. \tag{S20}$$

Remarkably, for small SOC the amplitude of MAAR in a half-metal/S junction is determined solely by the strength of the SOC parameters λ_α and λ_β . This is what we call in the manuscript the universal behavior.

SPIN-ORBIT COUPLING EFFECTS ON THE CONDUCTANCE

In the manuscript we show the conductance at a fixed SOC for different spin polarizations P . Here we show the impact of SOC, in Fig. S1, on the conductance spectrum. For a metallic point contact ($Z = 0$) spin-flip AR is inhibited. Increasing SOC decreases the conductance in F. In half metals this leads to a zero subgap conductance, as the only contribution would come from spin-flip AR. For finite Z and SOC, spin-flip AR is present and the conductance exhibits a nonmonotonic dependence on the SOC strength. The conductance first increases with increasing SOC and then decreases again (insets in Fig. S1). At the

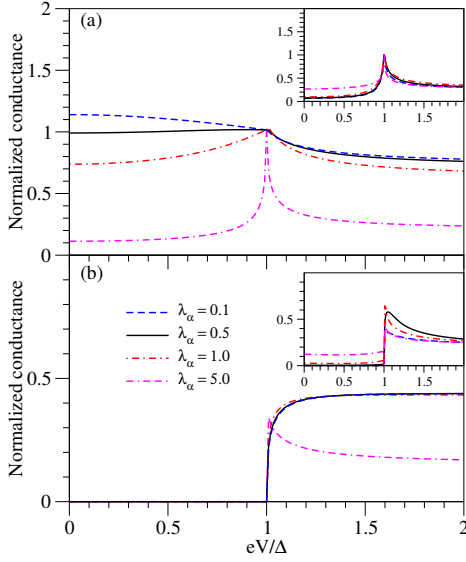


FIG. S1. Calculated dependence of normalized conductance on bias voltage for different strengths of Rashba SOC λ_α and Dresselhaus SOC $\lambda_\beta = 0$ in an ideal system $F_K = F_M = 1$. The magnetization is in-plane ($\Theta = \pi/2$). Panel (a) shows the results for a ferromagnetic system ($P = 0.4$) and panel (b) for a half-metallic ferromagnet ($P = 1$) in the absence of an interfacial barrier ($Z = 0$). In the insets a moderate interfacial barrier is present ($Z = 1$).

gap edge, the conductance is not affected by SOC at any Z .

MAAR VS TAMR

The presence of superconductivity makes MAAR remarkably different from its normal-state analog of tunneling anisotropic magnetoresistance, TAMR. The most important is the giant enhancement, as seen in Fig. 4 of the manuscript. A more subtle difference appears in the symmetry pattern of MAAR. In the manuscript we show (see Fig. 3 of the manuscript) that the interplay of Rashba and Dresselhaus SOC induces characteristic C_{2v} patterns of in-plane MAAR. If we also include a mismatch of the effective masses (say, if F is a ferromagnetic semiconductor), there can appear side lobes, while preserving the symmetry. An example for $F_M = 5$, in comparison with $F_M = 1$ is shown in Fig. S2(a). Side lobes may also appear in TAMR, but at much greater SOC magnitudes.

A comparison between the barrier strength dependences of MAAR and the corresponding TAMR ($\Delta = 0$) is shown in Fig. S2(b, c). The maximum value of MAAR and TAMR for a finite barrier occurs at slightly differ-

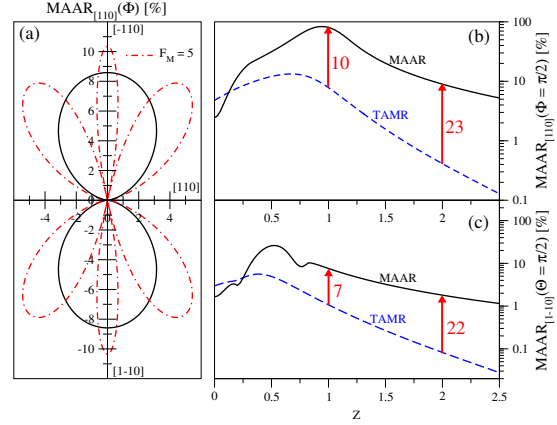


FIG. S2. Left: Formation of side lobes due to finite mass mismatch, $F_M = 5$ (dashed dotted line) for $Z = 1$, $P = 0.4$, $V = 0$ and $\lambda_\alpha = \lambda_\beta = 0.5$. Solid line is for the no mismatch, $F_M = 1$ case. Right: MAAR as a function of the barrier strength Z . On the top is the in-plane MAAR ($\lambda_\alpha = \lambda_\beta = 1$), on the bottom is the out-of-plane MAAR ($\lambda_\alpha = 1, \lambda_\beta = 0$). In both cases spin-polarization is $P = 0.4$, $V = 0$, and there is no lattice mismatch.

ent values of Z . This leads to a notable enhancement of the anisotropy in FS junctions with moderate Z with respect to TAMR. More remarkably, the MAAR amplitude can further be enhanced by orders of magnitude by increasing the spin polarization P , as discussed in detail in the manuscript. The experimentally measured in-plane TAMR in junctions with a single metallic F region is less than 1% [1]. In comparison to the measured TAMR values, the MAAR amplitudes at $P \gtrsim 50\%$ can be considered giant.

MAAR VS TAMR: A PHENOMENOLOGICAL APPROACH

As discussed above, MAAR and TAMR behave in qualitatively different ways with respect to changes of system parameters such as SOC strength, barrier strength, or effective mass (Fermi wave vector) mismatch. To understand the physical origin of such differences we use a simple phenomenological model proposed earlier for TAMR [2, 3]. Based on general symmetry considerations, this model predicts that, up to the second order in the SOC strength, the tunneling conductance has the form,

$$G(\Phi) \approx G^{(0)} + G_{so}(\Phi), \quad (S21)$$

where $G^{(0)}$ is the SOC-independent part of the conductance. The SOC-dependent part can be decomposed as

$$G_{so}(\Phi) = G_{so}^{iso} + G_{so}^{aniso}(\Phi), \quad (S22)$$

where

$$G_{so}^{iso} \propto (\lambda_\alpha^2 + \lambda_\beta^2) \quad (S23)$$

and

$$G_{so}^{aniso}(\Phi) \propto 2\lambda_\alpha\lambda_\beta \cos(2\Phi) \quad (S24)$$

are, respectively, the isotropic and anisotropic parts of G_{so} . The in-plane TAMR is then given by,

$$\text{TAMR}_{[110]}(\Phi) = \frac{G_{so}^{aniso}(0) - G_{so}^{aniso}(\Phi)}{G^{(0)} + G_{so}(\Phi)}. \quad (S25)$$

In TAMR junctions interfacial SOC is a perturbative effect and the conductance is largely dominated by its SOC-independent part, i. e., $G^{(0)} \gg G_{so}(\Phi)$. The TAMR can then be expanded as,

$$\begin{aligned} \text{TAMR}_{[110]}(\Phi) = & \quad (S26) \\ \frac{G_{so}^{aniso}(0)[1 - \cos(2\Phi)]}{G^{(0)}} & \left[1 - \frac{G_{so}^{aniso}(0) \cos(2\Phi)}{G^{(0)}} + \dots \right]. \end{aligned}$$

Here we took into account that $G_{so}^{aniso}(\Phi) = G_{so}^{aniso}(0) \cos(2\Phi)$. Since $G^{(0)} \gg G_{so}^{aniso}$, the in-plane TAMR is typically a small effect exhibiting an “8”-shaped angular dependence,

$$\text{TAMR}_{[110]}(\Phi) \approx \frac{G_{so}^{aniso}(0)[1 - \cos(2\Phi)]}{G^{(0)}}. \quad (S27)$$

For the formation of side lobes higher order terms in the expansion in Eq. (S26) must be sizable and this occurs only for considerably large values of the SOC strength, for which G_{so}^{aniso} starts to be comparable to $G^{(0)}$.

The situation is qualitatively different in the case of FS junctions, since here $G^{(0)}$ decreases when the spin polarization of the ferromagnetic lead increases. Thus, when the spin polarization is large enough and large effective mass mismatch [see Fig. S2(a)] is present, $G^{(0)}$ can be comparable and even smaller than G_{so}^{aniso} . In such a situation higher order terms in the expansion in Eq. (S26) can become relevant even when SOC is weak. This explains why in FS junctions with weak SOC the angular dependence of the MAAR exhibits side lobes, while they are absent in the TAMR.

When the half-metallic limit is reached, the only mechanism available for the subgap conductance is the spin-flip AR, which is determined by SOC. Therefore for half-metal/S junctions $G^{(0)}$ vanishes and the analog to Eq. (S25) reads as,

$$\text{MAAR}_{[110]}(\Phi) = \frac{G_{so}^{aniso}(0) - G_{so}^{aniso}(\Phi)}{G_{so}(\Phi)}. \quad (S28)$$

The approximate relation of the MAAR previously obtained in Eq. (S19) can now be reproduced by substituting Eqs. (S23) and (S24) into (S28).

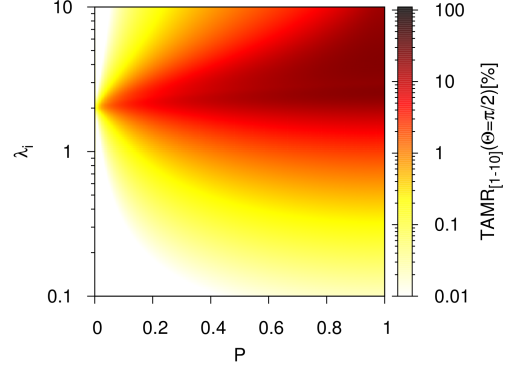


FIG. S3. Color map of the magnitude of out-of-plane TAMR at $\Theta = \pi/2$ for $V = 0$ and $Z = 1$ as a function of spin polarization and SOC strength λ_i with $i \in \{\alpha, \beta\}$.

Since the denominator in Eq. (S25) is determined by $G^{(0)}$, the size of the in-plane TAMR is fundamentally limited by the value of the SOC-independent part of the tunneling conductance. On the contrary, the MAAR in half-metal/S junctions can in principle be largely enhanced by making G_{so} in the denominator of Eq. (S28) sufficiently small. As mentioned above, the only mechanism available for the conductance in half metals when the energy resides inside the superconducting gap is the spin-flip AR. Spin flip is however suppressed when the interfacial SOC field, \mathbf{w} , and the magnetization orientation, \mathbf{m} , are collinear. Such a situation is not typical because the direction of the SOC is, in general, determined by the carriers wave vectors [see Eq. (S3)]. Yet, when $\lambda_\alpha = \lambda_\beta$ ($\lambda_\alpha = -\lambda_\beta$) the SOC field aligns along the \mathbf{y} [$\bar{1}10$] (\mathbf{x} \parallel $[110]$) direction, independently of the direction of \mathbf{k} [see Eq. (S3)]. Consequently, when $\lambda_\alpha = \lambda_\beta$ ($\lambda_\alpha = -\lambda_\beta$) and $\Phi = \pi/2$ ($\Phi = 0$), $\mathbf{w} \parallel \mathbf{m}$, and the spin-flip AR is strongly suppressed. Under these conditions, the denominator in Eq. (S28) becomes vanishingly small and the MAAR_[110]($\Phi = \pi/2$) is largely enhanced. This complements our discussion of the giant MAAR in the manuscript.

In the out-of-plane configuration, magnetoanisotropy is also present if the system contains only Rashba or Dresselhaus SOC. As discussed in the manuscript, for moderate SOC ($\lambda_i \lesssim 1$) the out-of-plane MAAR in half metals is independent of the SOC strength and shows a universal amplitude of 100%. This universality is absent for out-of-plane TAMR (Fig. S3). We can again use the phenomenological model to understand the reason for this. Analogously to Eqs. (S21-S24) we write the conductance as

$$G(\Theta) \approx G^{(0)} + G_{so}(\Theta) \quad (S29)$$

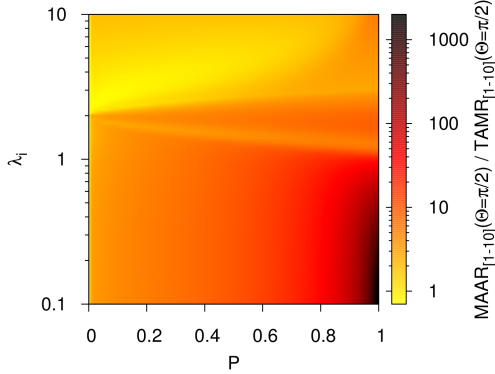


FIG. S4. Color map of the ratio of out-of-plane MAAR/TAMR at $\Theta = \pi/2$ for $V = 0$ and $Z = 1$ as a function of spin polarization and SOC strength λ_i with $i \in \{\alpha, \beta\}$.

and decompose the SOC-dependent part as

$$G_{so}(\Theta) = G_{so}^{iso} + G_{so}^{aniso}(\Theta), \quad (S30)$$

where

$$G_{so}^{iso} \propto 3\lambda_i^2 \quad (S31)$$

and

$$G_{so}^{aniso}(\Theta) \propto \lambda_i^2 \cos(2\Theta). \quad (S32)$$

λ_i with $i \in \{\alpha, \beta\}$ denotes Rashba or Dresselhaus SOC parameter, respectively. The out-of-plane TAMR is

$$\begin{aligned} \text{TAMR}_{[1\bar{1}0]}(\Theta) &\approx \frac{G_{so}^{aniso}(0)[1 - \cos(2\Theta)]}{G^{(0)}} \quad (S33) \\ &\propto \frac{\lambda_i^2[1 - \cos(2\Theta)]}{G^{(0)}}. \end{aligned}$$

For the MAAR we get

$$\begin{aligned} \text{MAAR}_{[1\bar{1}0]}(\Theta) &= \frac{G_{so}^{aniso}(0) - G_{so}^{aniso}(\Theta)}{G_{so}(\Theta)} \quad (S34) \\ &\approx \frac{1 - \cos(2\Theta)}{3 + \cos(2\Theta)}. \end{aligned}$$

The size of the out-of-plane TAMR is determined by the ratio of SOC strength λ_i^2 and $G^{(0)}$ since $G^{(0)} \gg G_{so}(\Theta)$.

Thus TAMR increases with increasing SOC. On the contrary, the out-of-plane MAAR ratio in half metals is independent of SOC for weak SOC. Since only spin-flip AR contributes to the conductance, $G^{(0)}$ is suppressed and $G_{so}(\Theta)$ becomes important. Therefore, both the denominator and numerator in Eq. (S34) are proportional to SOC parameters and the SOC dependence cancels out for a half-metal/S junction with either Rashba or Dresselhaus SOC. This leads to a universal MAAR of 100% corresponding to $G(\Theta = 0) = 2G(\Theta = \pi/2)$, i. e., for an incoming electron with out-of-plane spin the probability for spin-flip is twice as large as for an electron with in-plane spin. If only one of both considered SOC parameters is finite the SOC field lies in the \mathbf{x}, \mathbf{y} -plane and is isotropic with respect to Φ . Hence, for out-of-plane spin in \mathbf{z} direction two directions (\mathbf{x} and \mathbf{y}) exist, in which it can flip. Whereas, for an in-plane spin, e. g., in \mathbf{x} direction, only spin flip in one (\mathbf{y}) direction is possible leading to the typical ratio of out-of-plane and in-plane spin-flip ratios of 2 : 1. Since in half metal the conductance is solely determined by spin-flip mechanism, this ratio can directly be verified in the MAAR amplitude.

A fully numerical calculation of out-of-plane TAMR is presented in Fig. S3. Compared with Fig. 4. of the manuscript it is clear that MAAR is in general much greater. The corresponding ratio of out-of-plane MAAR/TAMR is in Fig. S4. The giant enhancement occurs for SOC parameters $\lambda_i \lesssim 1$, that is, in the perturbative regime, in accordance to our analytical calculations. Particularly strong is the enhancement in the half-metallic regime, $P \gtrsim 0.8$, in which out-of-plane MAAR is two orders of magnitude greater than out-of-plane TAMR.

-
- [1] J. Moser, A. Matos-Abiadue, D. Schuh, W. Wegscheider, J. Fabian, and D. Weiss, Phys. Rev. Lett. **99**, 056601 (2007).
 - [2] J. Fabian, A. Matos-Abiadue, C. Ertler, P. Stano, and I. Žutić, Acta Phys. Slov. **57**, 565 (2007).
 - [3] A. Matos-Abiadue and J. Fabian, Phys. Rev. B **79**, 155303 (2009).